# The Bright Optical Flash and Afterglow from the Gamma-Ray Burst GRB 130427A

W. T. Vestrand *et al.*

*Science* **343**, 38 (2014);
DOI: 10.1126/science.1242316



*Science* (print ISSN 0036-8075; online ISSN 1095-9203) is published weekly, except the last week in December, by the American Association for the Advancement of Science, 1200 New York Avenue NW, Washington, DC 20005. 

# The Bright Optical Flash and Afterglow from the Gamma-Ray Burst GRB 130427A

W. T. Vestrand,[1]* J. A. Wren,[1] A. Panaitescu,[1] P. R. Wozniak,[1] H. Davis,[1] D. M. Palmer,[1] G. Vianello,[2] N. Omodei,[2] S. Xiong,[3] M. S. Briggs,[3] M. Elphick,[4] W. Paciesas,[5] W. Rosing[4]

The optical light generated simultaneously with x-rays and gamma rays during a gamma-ray burst (GRB) provides clues about the nature of the explosions that occur as massive stars collapse. We report on the bright optical flash and fading afterglow from powerful burst GRB 130427A. The optical and >100–megaelectron volt (MeV) gamma-ray flux show a close correlation during the first 7000 seconds, which is best explained by reverse shock emission cogenerated in the relativistic burst ejecta as it collides with surrounding material. At later times, optical observations show the emergence of emission generated by a forward shock traversing the circumburst environment. The link between optical afterglow and >100-MeV emission suggests that nearby early peaked afterglows will be the best candidates for studying gamma-ray emission at energies ranging from gigaelectron volts to teraelectron volts.

Gamma-ray bursts (GRBs) of long duration are associated with the collapse of massive stars to form black holes (*1*) or rapidly spinning, highly magnetized neutron stars (*2*). This collapse is believed to eject collimated relativistic jets that, through internal dissipation processes and collisions with the surroundings, generate luminous outbursts of electromagnetic radiation that have been detected at radio frequencies to very high (gigaelectron volt) gamma-ray energies. Most of the outburst energy is emitted in the gamma rays. But starting with the first observations establishing that GRBs occur at cosmological distances (*3*), correlative optical observations, in particular, have proven themselves as important tools for unraveling the nature of GRB explosions. Here, we present observations of the optical flash and early afterglow for a nearby burst that is bright enough in very-high-energy gamma rays to allow a detailed comparison of the >100-MeV gamma-ray and optical light curves. These optical observations cover the critical early phases of the explosion, from the time interval before the event onset through the bright optical and prompt gamma-ray–emitting period and well into the early afterglow phase.

Starting on 27 April 2013 at 07:47:06.42 UTC (hereafter $T_0$), the Gamma Ray Burst Monitor (GBM) on the Fermi Satellite, the Burst Alert Telescope (BAT) on the Swift Satellite, and an armada of other space-based gamma-ray instruments detected the onset of a powerful GRB (*4*, *5*). This GRB, called GRB 130427A, had the largest gamma-ray fluence (~$2.7 \times 10^{-3}$ erg/cm$^2$ in the 20- to 1200-keV band) measured in more than 18 years of operation by Konus-Wind (*6*) and set a record for duration of the >100-MeV gamma-ray–emitting interval (*5*). Spectroscopy of the optical counterpart (*7*), coarsely localized by the Swift BAT and later refined by follow-up with optical telescopes, places the GRB at a redshift $z = 0.34$, a distance about five times closer than the typical GRB localized by Swift. However, even accounting for its proximity, the intense gamma-ray fluxes observed imply an apparent isotropic energy release of nearly $10^{54}$ ergs and rank 130427A among the more powerful GRBs ever detected (*3*). Subsequent optical monitoring revealed the emergence of a broad-line supernova at the GRB location (*8*).

### The Bright Optical Flash

This powerful GRB also generated an extremely bright flash of optical emission and a long-lived, bright optical afterglow. Three independent RAPTOR (Rapid Telescopes for Optical Response) full-sky monitoring telescopes (*9*), at locations in New Mexico and Hawaii, detected the emergence of a bright flash, temporally coincident with the onset of gamma-ray emission, at the location of GRB 130427A. The optical flash rapidly peaked at a magnitude of 7.03 ± 0.03 (unfiltered observations calibrated to Sloan r′ band) in an exposure that covered the time interval from $T_0 + 9.31$ s to $T_0 + 19.31$ s. After the peak, the flash faded with a power-law flux decay with index $\alpha = -1.67 \pm 0.07$ ($\chi^2 = 0.68/5$ degrees of freedom) and was detected for ~80 s until it faded below the ~10th magnitude sensitivity limit of the RAPTOR full-sky monitors.

The taxonomy for optical emission detected during the prompt gamma-ray emitting interval identifies two broad classes: prompt optical emission correlated with prompt gamma-ray emission (*10*–*12*) and early optical afterglow emission uncorrelated with the prompt gamma-ray emission (*11*, *13*, *14*). In context of the standard fireball model (*15*, *16*), the prompt optical emission is attributed to internal shocks in an ultrarelativistic jet outflow generated by the central engine and the afterglow emission to external shocks generated by interaction with the surrounding medium. The prompt optical emission therefore reflects the impulsive energy injection into the jet, and the early afterglow emission measures the response of the jet-environment system to the energy injection. Bright optical flashes from reverse shocks were predicted on theoretical grounds (*16*, *17*) before observational evidence was seen in GRB 990123

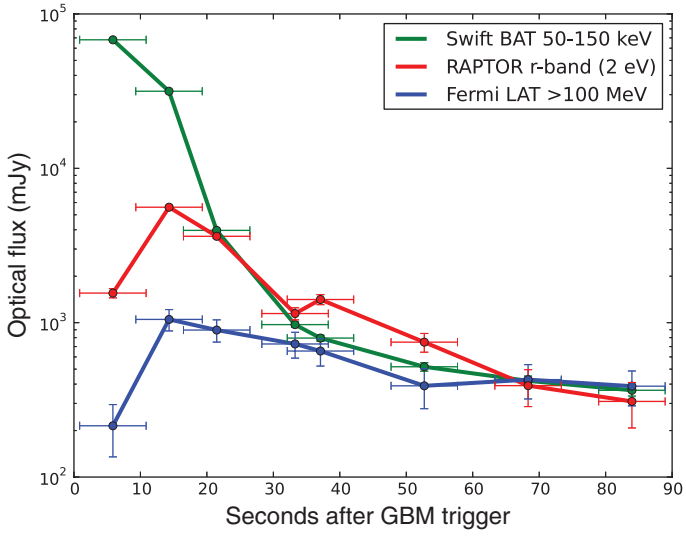


**Fig. 1. A comparison of the relative flux variations measured for GRB 130427A by the Fermi LAT, RAPTOR, and the Swift BAT during the first 90 s after the GRB trigger.** The >100-MeV emission and the 50- to 150-keV emission have been integrated over the same time intervals as the optical exposures and multiplied by a scaling factor to allow comparison with the optical light curve. Both the optical and >100-MeV light curves rise to a peak in the second interval, 50- to 150-keV emission peaks in the first interval. Horizontal error bars denote the time interval for the measurement; vertical error bars denote the 1σ uncertainty on the measured flux density.

[1]Los Alamos National Laboratory, P.O. Box 1663, Los Alamos, NM 87545, USA. [2]W.W. Hansen Experimental Physics Laboratory, Kavli Institute for Particle Astrophysics and Cosmology, Department of Physics, and SLAC National Accelerator Laboratory, Stanford University, Stanford, CA 94305, USA. [3]Center for Space Plasma and Aeronomic Research, University of Alabama in Huntsville, 320 Sparkman Drive, Huntsville, AL 35899, USA. [4]Las Cumbres Observatory Global Telescope Network, 6740 Cortona Drive, Suite 102, Santa Barbara, CA 93117, USA. [5]Universities Space Research Association, 320 Sparkman Drive, Huntsville, AL 35899, USA.

*Corresponding author. E-mail: vestrand@lanl.gov

(*13*). The optical flash light curve for GRB 130427A shows a single peak delayed with respect to the kiloelectron volt–megaelectron volt (keV-MeV) prompt gamma-ray peak (Fig. 1) and a steep power-law flux that is consistent with the predictions of models for optical flashes from reverse shocks (*17*). Based on the above taxonomy, the brightness of the flash, and the rapid power-law flux decay, it makes sense to associate the optical flash with reverse shock emission.

To explore the evolution of the broadband GRB spectrum during the optical flash, we used simultaneous measurements taken with the Fermi GBM and the Fermi Large Area Telescope (LAT) to construct spectral energy distributions (SEDs). Each snapshot of the time-evolving SED was formed by integrating the GRB flux over the same time interval as the optical exposure. We found that the broadband SEDs (Fig. 2) varied rapidly during the first 40 s, and the optical measurements fell far from the values expected from extrapolation of the keV-MeV SED. However, as the intensity of the outburst declined during the next 40-s interval, the SED shape stabilized, and the optical measurements

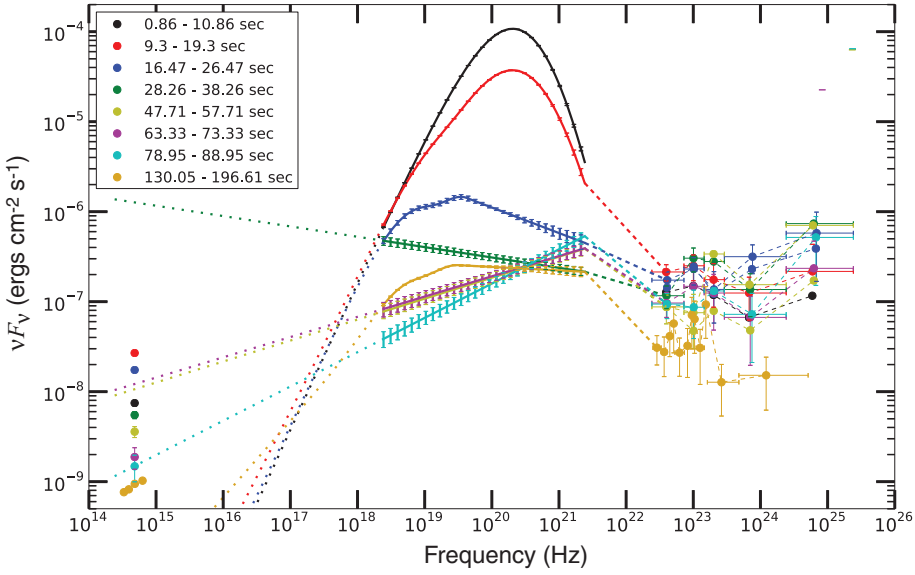


**Fig. 2. The spectral energy distributions measured for GRB 130427A during the early phases of the burst development.** The points and solid lines represent actual measurements. The dotted straight lines indicate the extrapolation the keV-MeV measurements for comparison to the optical measurements. The dashed lines indicate the connection between energy bands and are not actual measurements. The measurements were obtained by RAPTOR, the Fermi GBM, and the Fermi LAT. The vertical errors bars (indicating the 1σ confidence interval) on the GBM measurements have been increased by 25% to allow for systematics, such as pulse pile-up, background subtraction during and after the repointing of Fermi, and the rapid spectral evolution during the exposure intervals. $\nu F_\nu$ is the energy flux measured at a given frequency. The horizontal error bars on the values at very high frequencies denote the frequency interval for the energy flux measurement.

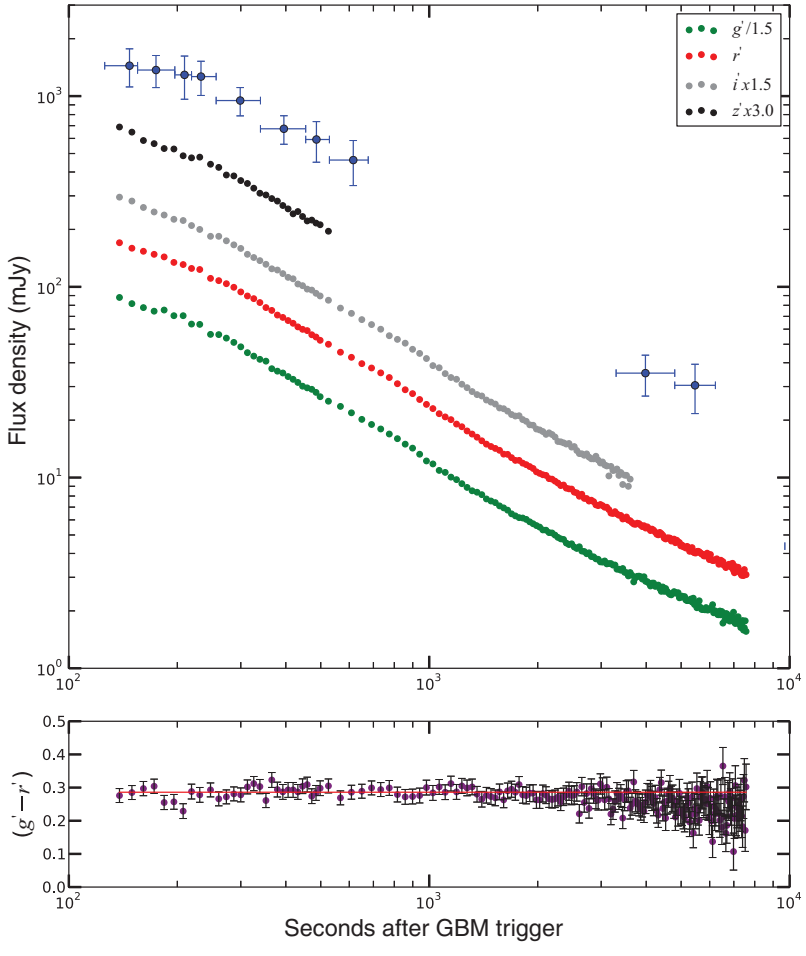


**Fig. 3. Simultaneous multicolor measurements of the early optical afterglow from GRB 130427A.** (**Top**) Light curves obtained using standard Sloan g′, r′, i′, and z′filters (*24*). The light curves show more structure than is captured by power-law fits, but the r′-band light curve can be characterized as a power-law decay with index ~0.7 before 270 s, ~1.1 between 270 and 3000 s, and 0.88 between 3000 and 7500 s. Also plotted for comparison, in blue, is the photon flux light curve for >100-MeV emission measured by the Fermi LAT (*4*). (**Bottom**) The g′-r′ color evolution of GRB 130427A. The red line indicates the mean g′-r′ value (0.286 ± 0.018) measured before $T_0$ + 1000 s. After about $T_0$ + 3000 s, a bluer component emerges as the flux decay slows. Vertical error bars indicate the 1σ (or 68%) confidence interval on the measured quantity; horizontal error bars, when long enough to be visible, denote the measurement time interval.

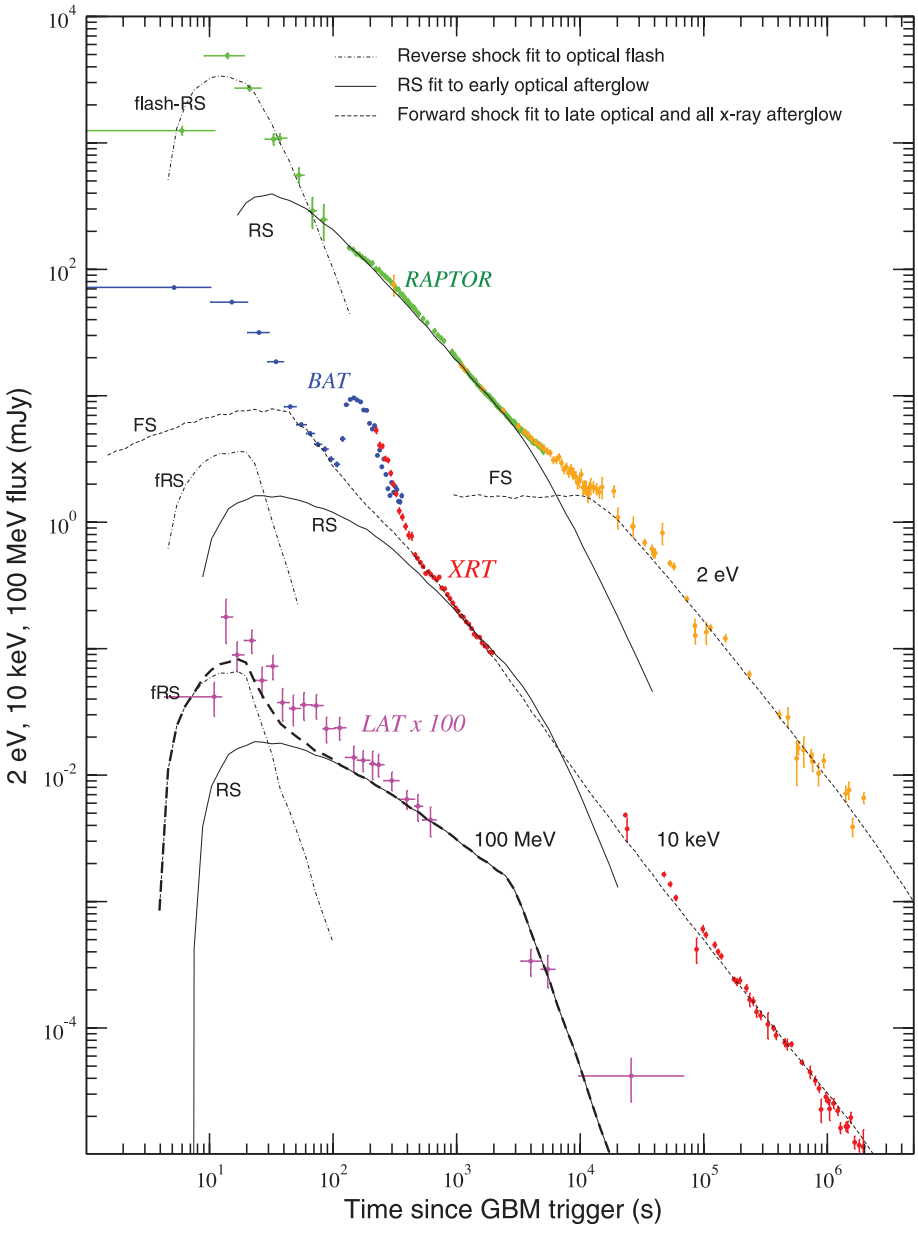


**Fig. 4. Best-fit with a reverse forward shock model to the optical light curve of GRB afterglow 130427A.** Three episodes of ejecta and energy injection are needed to explain the optical flash, the early optical emission (up to few kiloseconds), and the late optical emission (after a few kiloseconds). Here, each injection episode represents a change in the dynamical and microphysical parameters of the reverse shock in an otherwise continuous ejecta injection into the reverse shock. For the first two episodes, the optical emission arises from the reverse shock, and the kinetic energy of the incoming ejecta ($6.10^{52}$ erg/sr and $4.10^{53}$ erg/sr, respectively) is less than that of the leading shock ($10^{54}$ erg/sr). During the last injection episode, the optical afterglow emission arises from the forward-shock, with the incoming ejecta carrying $3.10^{54}$ erg/sr, which is more than that already existing in the forward shock (thus, its deceleration is mitigated by the energy injection). Other parameters are (i) first injection episode, flash reverse shock (fRS) onset at 4 s, end at 15 s, incoming ejecta Lorentz factor 730, magnetic field parameter 0.008, electron-energy parameter 0.006, index of electron power-law distribution with energy 1.9; (ii) second injection episode, reverse shock (RS, parameters in same order as above): 15 s, 3 ks, 1800, 0.0010, 0.012, 2.0; and (iii) third injection episode, forward shock (FS): 3 ks, >2 Ms, >100, $3.10^{-4}$, 0.14, 2.3, energy injection law $E \sim t^{0.3}$. The microphysical parameters for the forward shock are kept constant throughout the entire course of the event. We also require that the ambient medium have a windlike density stratification ($n \sim r^{-2}$, where $n$ is the wind density in particles per unit volume, and $r$ is the distance from the wind origin) corresponding to a GRB progenitor with a mass-loss rate–to–wind-speed ratio of $4.10^{-11}$ [units of (solar mass/year)/(km/s)]. Dot-dash lines show the model fits for the flash-phase emission, the solid lines show the reverse shock contributions during the early afterglow phase, and the dashed lines shows the contributions of the forward shock emission to the late optical afterglow and all phases of the x-ray afterglow. The reverse shock emission during the third injection episode is not shown and would be dimmer than that of the forward shock, if the reverse shock has the same microphysical parameters as the forward shock.

started to converge on the values predicted by a straightforward linear extrapolation of the keV-MeV SED. By the end of the optical flash, the optical–to–10-MeV spectrum is consistent with a single power law with index $\beta = -0.64$.

### Sustained External Shocks and High-Energy Gamma Rays

In response to the Swift BAT localization alert at 127.8 s after the GBM trigger, our RAPTOR response telescopes began unfiltered and simultaneous multicolor (g′, r′, i′, z′) optical observations at $T_0$ + 132.9 s that continued until $T_0$ + 7585.9 s. This photometry begins near the peak of a prominent flare in keV-MeV x-rays and gamma rays that lasts until ~$T_0$ + 400 s. The optical light curves show a smooth monotonic decline but no indication of the steep decline nor the break to a slower power-law decay at ~400 s measured at x-ray energies (*4*). Instead, the structure of the optical light curve shows a steepening at about $T_0$ + 270 s. This steepening is essentially achromatic, and the color of the optical emission is consistent with a $\nu^{-0.70 \pm 0.05}$ spectrum and is constant until it starts to become bluer ($\nu^{-0.59 \pm 0.05}$) at ~3000 s after the GBM trigger (see bottom panel of Fig. 3).

In marked contrast to the keV-MeV emission, the optical light curves after $T_0$ + 100 s show a strong similarity to the >100-MeV photon flux light curve measured by the Fermi LAT (*5*). The LAT light curve has a break at ~300 s, just like the optical afterglow. Straightforward scaling of the RAPTOR optical light curve by a factor of ~$10^{-6}$ provides a reasonable description of the LAT observations out to ~$T_0$ + 7000 s. This close correspondence argues for a common origin of both components in external shocks.

The optical light curve until ~$T_0$ + 3000 s is best modeled by synchrotron emission from a reverse shock in a wind density profile. Most optical afterglows have been modeled with forward shocks in a homogeneous medium, but the peak brightness [~6 jansky (Jy)] and steep decay of the optical flash suggest origin in a reverse shock. The relative faintness of the radio afterglow peak (~1 mJy) also argues for generation by a reverse shock in a windlike medium (*18*). To explain the optical flash by reverse shock emission in a wind ($R^{-2}$) requires either a long-lived electron-energy injection up to ~40 s or a shorter one (~20 s), followed by adiabatic cooling. Figure 4 shows the best fit to the optical flash with the short interval of injection (on at $T_0$ + 4 s and off at $T_0$ + 20 s) and, for self-consistency, the same dynamical parameters that we infer from fits to the later afterglow forward shock emission discussed below.

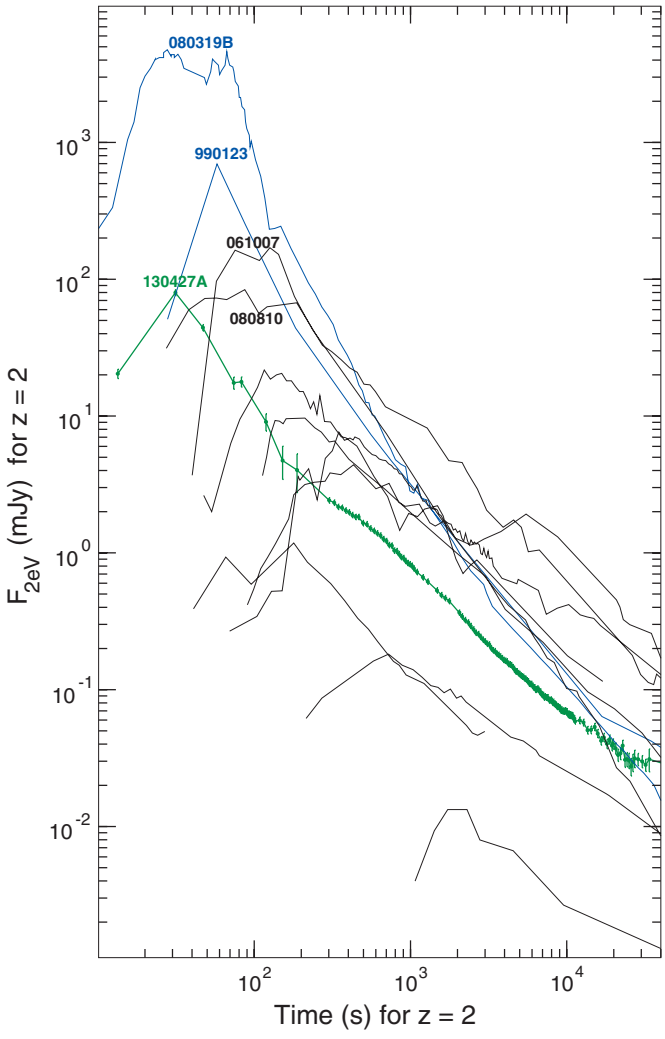


**Fig. 5. Comparison of the light curve from GRB 130427A (in green) with those measured for other prominent GRBs with peaked optical afterglows.** All of the light curves have been transformed to show how they would appear if they had occurred at redshift $z = 2$. $F_{2eV}$, flux density at 2 eV.

This model employs an electron distribution with power-law energy index $p = 1.88$ and corresponds to an injected energy of $8.0 \times 10^{53}$ ergs. The slower optical fading after the flash interval requires a second episode of energy injection to sustain the optical afterglow or a continuous outflow with a variable Lorentz factor (*19*). This sustained reverse shock model reproduces the closely tracking variability observed by the RAPTOR telescopes and the Fermi LAT and suggests that the optical emission, and most of the >100-MeV emission, is generated by synchrotron emitting electrons that are accelerated by the reverse shocks.

By itself, this reverse shock model cannot explain the properties of the prompt keV-MeV emission, nor some of the properties of the late-time afterglows. The evolution to a bluer color after ~3000 s observed by RAPTOR and the slowing of the optical brightness decay suggest the emergence of a forward shock component. This transition to forward shock dominance at late times would also naturally explain the late-time x-ray light curve and the sustained >100-MeV emission after 10,000 s. Emergence of a bluer optical component at late times is similar to the afterglow evolution of GRB 080319B—another burst with a bright optical flash. For GRB 080319B, the color change was also interpreted as marking the transition from reverse shock emission dominance to forward shock dominance (*12*, *20*, *21*).

During most of the interval before $T_0 + 400$ s, the keV-MeV x-ray and gamma-ray emission is consistent with the standard assumption that the prompt emission is generated by internal shocks in the relativistic jet ejecta. Our predicted >100-MeV flux from the reverse shock that generates the optical flash is slightly less (about a factor of 2) than the peak measured by the Fermi LAT (Fig. 4). But the keV-MeV flux is substantially underpredicted by at least a factor of 10, so the reverse shock in a wind model requires prompt emission to explain the keV-MeV emission and might require additional >100-MeV emission to explain the LAT light-curve peak. In this picture, the keV-MeV light curve is a proxy that traces the injection of internal jet energy by the central engine. The keV-MeV emission therefore indicates two periods of substantial energy injection into the jet: the initial 20 s and a period from ~120 to 300 s. The interesting potential exception to prompt emission dominance in the keV-MeV range is the period just before onset of the flare at $T_0 + 120$ s. During the interval $T_0 + 79$ s to $T_0 + 89$ s, the optical afterglow flux measured by RAPTOR falls right on the extrapolation of the power law (index = ~−0.6) measured by the GBM in the energy band from 10-keV to 20-MeV. This gamma-ray spectral slope is also similar to spectral slope that we measure for optical afterglow emission at later times. The notch in the keV-MeV light curve before the flare at $T_0 + 120$ may be providing a rare glimpse, similar to that seen in GRB 980923 (*22*), of afterglow emission at megaelectron volt energies between prompt emission intervals.

The exceptional optical properties observed for the optical flash and afterglow from GRB 130427A are mostly a result of burst proximity. The flash peak luminosity for GRB 130427A is among the most powerful events, but its value is consistent with the anticorrelation between peak time and peak luminosity (Fig. 5) found for optical afterglows (*23*). If optical afterglows and >100-MeV gamma-ray afterglows have a common origin, then the optical afterglows that peak early should be the best candidates for detection at gigaelectron volt–teraelectron volt gamma-ray energies.

## References and Notes


1. S. E. Woosley, J. S. Bloom, *Annu. Rev. Astron. Astrophys.* **44**, 507–556 (2006).
2. B. D. Metzger, D. Giannios, T. A. Thompson, N. Bucciantini, E. Quataert, *Mon. Not. R. Astron. Soc.* **413**, 2031–2056 (2011).
3. M. R. Metzger *et al.*, *Nature* **387**, 878–880 (1997).
4. A. Maselli *et al.*, *Science* **343**, 48–51 (2014).
5. M. Ackermann *et al.*, *Science* **343**, 42–47 (2014).
6. S. Golenetskii *et al.*, "Konus-wind observation of GRB 130427A," GCN Circular 14486 (NASA, Greenbelt, MD, 2013).
7. A. J. Levan *et al.*, "GRB 130427A: Gemini-north redshift," GCN Circular 14455 (NASA, Greenbelt, MD, 2013).
8. D. Xu *et al.*, *Astrophys. J.* **776**, 98 (2013).
9. J. Wren, W. T. Vestrand, P. Wozniak, H. Davis, *Proc. SPIE* **7737**, 773723 (2010).
10. W. T. Vestrand *et al.*, *Nature* **435**, 178–180 (2005).
11. W. T. Vestrand *et al.*, *Nature* **442**, 172–175 (2006).
12. J. L. Racusin *et al.*, *Nature* **455**, 183–188 (2008).
13. C. Akerlof *et al.*, *Nature* **398**, 400–402 (1999).
14. E. Rykoff *et al.*, *Astrophys. J.* **702**, 489–505 (2009).
15. P. Meszaros, M. Rees, *Astrophys. J.* **405**, 278–284 (1993).
16. P. Meszaros, M. Rees, *Astrophys. J.* **476**, 232–237 (1997).
17. R. Sari, T. Piran, *Astrophys. J.* **520**, 641–649 (1999).
18. T. Laskar, preprint available at http://arxiv.org/abs/1305.2453 (2013).
19. Z. L. Uhm *et al.*, *Astrophys. J.* **761**, 147 (2012).
20. P. Wozniak *et al.*, *Astrophys. J.* **691**, 495–502 (2009).
21. J. S. Bloom *et al.*, *Astrophys. J.* **691**, 723–737 (2009).
22. T. W. Giblin *et al.*, *Astrophys. J.* **524**, L47–L50 (1999).
23. A. Panaitescu, W. T. Vestrand, *Mon. Not. R. Astron. Soc.* **387**, 497–504 (2008).
24. The RAPTOR optical measurements are available in table S1 of the supplementary materials on *Science* Online.


**Acknowledgments:** This GRB research was supported by NASA and the Laboratory Directed Research and Development program at Los Alamos National Laboratory. The optical measurements reported in this paper are available online in the supplementary materials.

## Supplementary Materials

www.sciencemag.org/content/343/6166/38/suppl/DC1
Supplementary Text
Table S1
References (*25*–*31*)

24 June 2013; accepted 21 October 2013
Published online 21 November 2013;
10.1126/science.1242316